American Mineralogist, Volume 82, pages 483–496, 1997

XAFS spectroscopic study of uranyl coordination in solids and aqueous solution

HILLARY A. THOMPSON, GORDON E. BROWN JR., AND GEORGE A. PARKS

Department of Geological and Environmental Sciences, Stanford University, Stanford, CA 94305–2115, U.S.A.

ABSTRACT

To evaluate the ability of X-ray absorption fine structure (XAFS) spectroscopy to elucidate the coordination environment of U^{6+} at the solid-water interface, we conducted an in-depth analysis of experimental XAFS data from U^{6+} solid and solution model compounds. Using the ab initio XAFS code FEFF6, we calculated phase-shift and amplitude functions for fitting experimental data. The code FEFF6 does a good job of reproducing experimental data and is particularly valuable for providing phase-shift and amplitude functions for neighboring atoms whose spectral contributions are difficult to isolate from experimental data because of overlap of Fourier transform features. In solid-phase model compounds at ambient temperature, we were able to fit spectral contributions from axial O (1.8 Å), equatorial O (2.2–2.5 Å), N (2.9 Å), C (2.9 Å), Si (3.2 Å), P (3.6 Å), distant O (4.3 Å), and U (4.0, 4.3, 4.9, and 5.2 Å) atoms. Contributions from N, C, Si, P, distant O, and distant U (4.9 and 5.2 Å) are weak and therefore might go undetected in a sample of unknown composition. Lowering the temperature to 10 K extends detection of U neighbors to 7.0 Å. The ability to detect these atoms suggests that XAFS might be capable of discerning inner-sphere U sorption at solid aluminosilicate-water interfaces. XAFS should definitely detect multinuclear U complexes and precipitates. Multiple-scattering paths are minor contributors to uranyl XAFS beyond $k = 3$ Å^{-1}. Allowing shell-dependent disorder parameters (σ^2) to vary, we observed narrow ranges of σ^2 values for similar shells of neighboring atoms. Knowledge of these ranges is necessary to constrain the fit of XAFS spectra for unknowns. Finally, we found that structures reported in the literature for uranyl diacetate and rutherfordine are not completely correct.

INTRODUCTION

Uranium is a significant environmental contaminant, particularly at several U.S. weapons complex sites, where it is found in soils and sediments (U.S. Department of Energy 1995). In such environments, natural waters enhance the extent to which U reacts with the surfaces of soil particles (sorption) and also may provide solution constituents for U complexation. The structure and composition of the resulting sorption and solution complexes modulate U mobility. To understand and predict U mobility, we need information about the coordination chemistry of U in these complexes.

X-ray absorption fine structure (XAFS) spectroscopy provides interatomic distance (R) and coordination number (N) information, as well as a measure of local disorder (σ^2, a Debye-Waller–like term) relative to a selected central atom. Combined with coordination chemistry principles, XAFS spectroscopy can provide quantitative information about the coordination environment of the central atom. The theory and practice of XAFS spectroscopy have been described extensively elsewhere (Teo 1986; Brown et al. 1988; Stern 1988).

Several XAFS spectroscopic investigations have probed the coordination environment of U^{6+} (the dominant oxidation state in our applications) in solids, aqueous solutions, and mixed solid-solution systems of unknown structure and composition. Using samples of known composition and structure, it has been shown repeatedly that XAFS can detect the first two shells of neighboring atoms around U^{6+} [axial O (O_{ax}) and equatorial O (O_{eq}) or equatorial F] in solids and aqueous solutions (Karim et al. 1980; Knapp et al. 1984; Dent et al. 1992; Farges et al. 1992; Chisholm-Brause et al. 1994). In addition, Dent et al. (1992) and Allen et al. (1995) identified several more distant neighbors in samples of otherwise unknown structure. In this study we establish the accuracy with which XAFS can identify and determine the location of atoms in second and more distant coordination shells on the basis of well-characterized crystalline (and one aqueous) compounds with various compositions and structures.

Knowledge of the technique's limitations beyond the O_{eq} shell is critical for several reasons. In solutions, the nature of uranyl ligands affects U mobility, thus it would be valuable to distinguish whether third-shell atoms are C (as in carbonate), N (as in nitrate), or some other element or combination of elements. For solid-water interface studies, observing a contribution to the XAFS spectrum from an atom unique to the sorbent could determine the relationship of the adsorbate to the sorbent surface. Typically, the nearest neighbor to a sorbed U atom that

0003–004X/97/0506–0483$05.00

satisfies this criterion is a metal atom in the surface layer of the metal oxide solid. Some authors have observed contributions from Fe atoms in U XAFS spectra of U sorbed in an inner-sphere manner to iron oxide solids (Combes 1988; Manceau et al. 1992; Waite et al. 1994). XAFS studies of U sorption on lower atomic number (Z) oxides ($Z < 26$), however, have failed to demonstrate the presence of a metal atom unique to the sorbent [e.g., Si or Al in montmorillonite (Chisholm-Brause et al. 1994) or Si in silica colloids (Dent et al. 1992)] in the coordination environment of U. This failure raises the issue of whether Si or Al atoms were not detected because they were not present in the extended coordination sphere around U, or because XAFS simply could not detect them, despite their presence.

Both in aqueous solution and at the solid-water interface, the formation of multinuclear complexes is of interest as a precursor to solid phase formation. Two studies reported detection of uranyl multinuclear complexes by XAFS (implied by the presence of a U neighbor contribution in the U XAFS spectrum) (Dent et al. 1992; Allen et al. 1995). In U^{6+}-containing solids, nearest U neighbors are typically found 3.7–4.9 Å from the central U atom. It would be valuable to know whether U atoms within and beyond this distance range are detectable consistently by XAFS spectroscopy.

There are several reasons for not detecting certain atoms in the short-range U^{6+} coordination environment (out to ~ 7 Å) using XAFS spectroscopy. Low atomic number atoms are weak photoelectron scatterers, resulting in weak spectral contributions, particularly over extended distances. Considerable static disorder is typically associated with atoms that lie in the uranyl-equatorial plane, including O_{eq}. This can result in destructive interference of spectral components and therefore relatively weak XAFS contributions. Significant multiple-scattering (MS) paths that occur at distances similar to single-scattering paths, but with different phase functions, can also destructively interfere with single-scattering paths, further complicating interpretation of the spectrum. Hudson et al. (1996) found MS contributions to be significant in the uranyl extended XAFS (EXAFS) region, but that conclusion was based on a single spectrum. Each of these factors affects the ability of the XAFS technique to detect atom neighbors by varying degrees, depending on sample composition. Therefore, knowledge of the detection limits of the XAFS technique for various sample compositions is required for accurate interpretation of XAFS data.

Typically a least-squares fit is used to extract coordination information (N, R, and σ^2) from experimental XAFS data. Because of the possibility of reaching a false minimum in the fit, which would lead to incorrect coordination information, we require reasonable limits for N, R, and σ^2 against which to evaluate fit results, as well as realistic phase-shift and amplitude functions to include in the least-squares fit. Values of N and R can be constrained by knowledge of coordination chemistry of the element of interest. We are not capable of calculating or directly measuring values of σ^2 for complex systems such as uranyl, however, and because σ^2 is highly correlated with N, varying both simultaneously in a fit is likely to result in incorrect estimates of both. For this reason, we require a basis for constraining σ^2 values to fit XAFS data correctly for U in unknown environments.

Therefore, we undertook this study with several objectives. Using FEFF6 (Mustre de Leon et al. 1991; Rehr et al. 1991; Zabinsky et al. 1995) phase-shift and amplitude functions, we fitted experimental XAFS data to determine which neighboring atoms in the local atomic environment around U can be detected using XAFS and whether MS spectral contributions are significant. We evaluated data for three of the solid model compounds at low temperature (10 K) to determine the effect of temperature on detection limits and disorder parameters. Finally, we established reasonable ranges for σ^2 values for each coordination shell in the U^{6+} environment.

Materials and methods

The model compounds used in this study are listed with their chemical formulas in Table 1. They fall into two structural groups: isolated or weakly associated uranyl units and layered uranyl structures. The uranyl moiety surrounded by four to six O_{eq} atoms forms the basic unit for both (Fig. 1a). In the former group, which includes the aqueous uranyl monomer, uranyl diacetate, and uranyl nitrate, hydrogen bonding connects the basic unit to H_2O molecules (aqueous monomer) or other uranyl units (uranyl nitrate) to form a relatively loose array. In the other group, ionic bonding joins the uranyl groups through their O_{eq} atoms and intervening atoms (C, Si, P) to one another to form planar arrays (Fig. 1b). The planes stack to form layered structures, as in rutherfordine, uranophane, meta-autunite, and meta-ankoleite.

Our model compounds consisted of reagent grade chemicals and natural minerals. Uranyl nitrate (hexahydrate) and uranyl diacetate were reagent grade chemicals obtained from J.T. Baker Chemical Co. The origins of our rutherfordine and uranophane are unknown. Meta-autunite came from the Margnac Mine, Haute Vienne, France (Smithsonian collection, no. 112882-1). Meta-ankoleite was synthesized by M. Barr of Los Alamos National Laboratory (LANL) by stepwise addition of KOH to a uranyl-phosphate solution. The boron nitride (BN) used as a diluent in preparation of solid model compound samples was from Aldrich Chemical Company.

Powder X-ray diffraction (XRD) data confirmed the identity and crystallinity of all solid model compounds by comparison with the Powder Diffraction File (Thompson 1994). Diffraction data for the nitrate, diacetate, and rutherfordine were obtained using Cu$K\alpha$ radiation (λ = 1.5418 Å) on a Rigaku powder X-ray diffractometer at Stanford University. Diffraction data for meta-autunite, meta-ankoleite, and uranophane were collected at LANL on a Phillips XRG3100 instrument using Cu$K\alpha$ radiation.

The solution model compound consisted of 0.05 M uranyl nitrate in doubly deionized water, with sufficient

TABLE 1. Coordination number (N), interatomic distance (R), disorder parameter (σ^2), and goodness-of-fit parameter (ϵ^2) for EXAFS fits and comparison with XRD data

Compound	EXAFS					XRD
	Atom	N*	R (Å)	σ^2 (Å^2)	ϵ^2	R (Å)
Aqueous uranyl ion	O_{ax}	2	1.77	0.0015	2.814	
0.05 M $UO_2(NO_3)_2$(aq)	O_{eq}	5	2.42	0.0092	2.137	
Uranyl diacetate	O_{ax}	2	1.77	0.0031	1.026	
$UO_2(CH_3CO_2)_2 \cdot nH_2O$(s)	O_{eq}	6	2.40	0.0127	0.460	
Uranyl nitrate	O_{ax}	2	1.76	0.0028	1.780	1.76
$UO_2(NO_3)_2 \cdot 6H_2O$(s)	O_{eq}	6	2.49	0.0100	0.895	2.48
	N	2	2.93	0.0101	0.988	2.96
Rutherfordine	O_{ax}	2	1.77(1.76)	0.0024(0.0030)	0.991(2.995)	1.67
UO_2CO_3(s)	O_{eq}	6	2.46(2.47)	0.0105(0.0070)	0.443(2.240)	2.46
	C	2	2.94(2.91)	0.0024(0.0031)	0.372(2.255)	2.86
	U1	2	4.31(4.30)	0.0061(0.0023)	0.283(1.084)	4.30
	O_{dist}	8	4.28(4.25)	0.0097(0.0057)	0.272(1.045)	4.37
	U2	2	4.88(4.87)	0.0064(0.0028)	0.255(0.730)	4.85
	U3	8	(5.58)	(0.0078)	(0.677)	5.64
	U4	4	(6.50)	(0.0036)	(0.583)	6.48
Uranophane	O_{ax}	2	1.82(1.82)	0.0019(0.0028)	1.776(5.421)	1.82[1.80]
$Ca(UO_2)_2(SiO_3OH)_2 \cdot 5H_2O$(s)	O_{eq1}	3	2.32(2.27)	0.0016(0.0027)	1.006(5.222)	2.30[2.28]
	O_{eq2}	2	2.49(2.43)	0.0020(0.0045)	0.658(5.338)	2.48[2.45]
	U1	2	3.96(3.93)	0.0054(0.0016)	0.466(1.679)	3.92[3.92]
	Si1	1	3.17(3.19)	0.0033(0.0013)	0.401(1.640)	3.16[3.14]
Meta-autunite	O_{ax}	2	1.77	0.0040	2.763	1.76
$Ca(UO_2)_2(PO_4)_2 \cdot 6H_2O$(s)	O_{eq}	4	2.28	0.0031	0.654	2.31
	P	4	3.60†	0.0153	0.628	3.60
Meta-ankoleite	O_{ax}	2	1.78(1.78)	0.0031(0.0031)	2.751(7.352)	1.76
$K_2(UO_2)_2(PO_4)_2 \cdot 6H_2O$(s)	O_{eq}	4	2.29(2.29)	0.0025(0.0024)	0.462(5.105)	2.31
	P	4	3.60†(3.61)	0.0043(0.0041)	0.452(4.986)	3.60
	U1	4	5.25(5.24)	0.0093(0.0018)	0.436(2.430)	5.24
	MS	1	3.71†	0.0026	0.268‡	3.71
	MS	1	4.61†	0.0036		4.61
	U2	4	(7.00†)	(0.0056)	(1.586)	7.00
	MS	1	(7.02†)	(0.0032)	(1.450)	7.00–7.04

Note: Ambient-temperature data appear first; 10 K data are in parentheses. β-uranophane XRD distances appear first; those for the α-polymorph appear in brackets. Representative standard deviations for R by shell (in Å) are 0.002 (O_{ax}), 0.004 (O_{eq}), 0.004–0.01 (U, increasing with $R_{U\text{-}U}$), 0.007 (Si), and 0.009 (other light atoms).

* N fixed to crystallographic value; see text.

† Parameter value held constant.

‡ ϵ^2 corresponds to the addition of two shells, the one marked and the following shell.

reagent grade nitric acid to reduce the pH of the solution to <1.0. Dissolution of the starting solid was visibly complete. These conditions ensured predominance of the monomeric $UO_2^{2+} \cdot 5H_2O$(aq) ion, on the basis of species distributions calculated using the computer code HYDRAQL (Papelis et al. 1988) and the NEA database of U thermodynamic data (Grenthe et al. 1992). Species identification was not independently verified using spectroscopic methods. Just before XAFS data collection, an aliquot of solution was injected into a 1.5 mm thick Teflon solution cell with Mylar windows using a syringe.

XAFS sample preparation

Solid model compounds were ground in an agate mortar and pestle and mixed with solid BN in proportions yielding 63% absorption of the incoming beam, or $\mu\rho x = 1$, where μ is the mass absorption coefficient of the sample (cm^2/g), ρ is the density of the sample (g/cm^3), and x is the thickness of the sample (cm) (McMaster et al. 1969). The mixture was pressed into a 0.5 mm thick aluminum sample holder between Mylar windows.

XAFS data collection

Uranium L_{III}-edge XAFS spectra (~17–18 keV; nominal edge inflection 17166 eV) were collected at the Stanford Synchrotron Radiation Laboratory (SSRL; 3 GeV and 40–90 mA) using beam lines IV-2 (ambient temperature) and II-3 (low T = 10 K). Low temperatures were maintained using an Oxford liquid He cryostat. The X-ray beam was unfocused on a Si(220) monochromator crystal (ϕ = 90°). Vertical slit apertures were set to 1.0 mm (monochromator, both beam lines) and 1.0 mm (hutch, 2.0 mm on II-3). Spectra were collected in transmission mode using Ar-filled ionization chambers. Harmonic rejection was effected by 10–80% detuning of the incident beam. Three to five scans were collected for each sample. A uranium oxide standard was mounted between two ionization chambers downstream from the sample to provide a continuous energy calibration reference.

XAFS data analysis

Details of the XAFS data analysis procedure that are specific to this study are given here. Numerous review articles provide more complete accounts (Cramer and

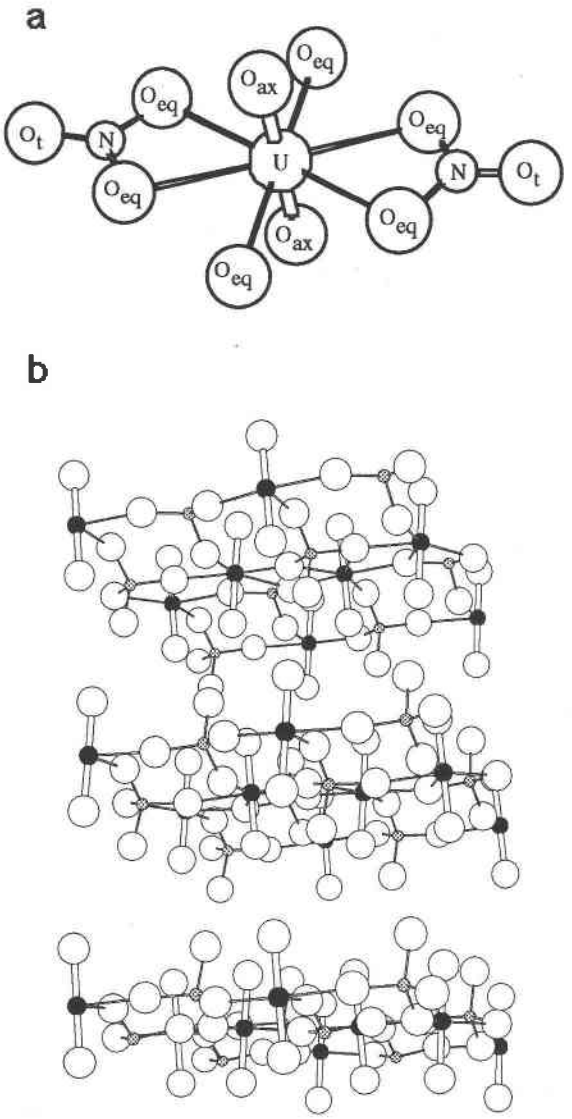

FIGURE 1. (**a**) Basic structural unit of uranyl nitrate. Different O atom environments are distinguished by axial (O_{ax}), equatorial (O_{eq}), and terminal (O_t) designations. Equatorial O atoms that are not bonded to N are part of H_2O molecules. (**b**) Extended layer structure of α-uranophane. Solid circle, represents U atoms, Shaded are Si, and open are O. Basic units similar to that shown in (**a**) are bonded together through U-O_{eq}-Si-O_{eq}-U linkages in uranophane. Linear uranyl moieties are approximately perpendicular to layers.

Hodgson 1979; Sayers and Bunker 1988). Unless otherwise stated, we conducted all of the data analysis using programs contained in EXAFSPAK, written by G. George of SSRL (George and Pickering 1993).

Raw spectra were calibrated individually by setting the position of the first inflection point of the calibration standard absorption edge equal to 17166 eV, the nominal L_{III}-edge energy for elemental uranium (Vaughan 1986). Calibrated scans for each sample were averaged together using weighting proportional to the square of the signal-to-noise ratio. First-order polynomials were fitted to pre-edge spectra and subtracted. Splines consisting of three or four regions of fourth-order polynomials, the number of regions depending primarily on the data range, were fitted to the EXAFS regions and subtracted. Resulting spectra were normalized using the absorption cross-section for U, measured at 17200 eV, which was extrapolated through the EXAFS region using the Victoreen equation (Scott 1984). Stack plots of resulting EXAFS ($k^3\chi$) spectra are included in Figures 2, 3, and 4. The EXAFS spectra were then transformed over the k range where data quality was high, but never starting below $k = 3$ Å^{-1}. Resulting Fourier transform (FT) spectra are also plotted in Figures 2, 3, and 4.

We used the program FEFF6 to calculate EXAFS spectra for uranyl nitrate (Taylor and Mueller 1965), rutherfordine (Cromer and Harper 1955), α-uranophane (Ginderow 1988) and hydrogen uranyl phosphate (isostructural with meta-autunite and meta-ankoleite) (Morosin 1978), from which we obtained reference phase-shift and effective scattering amplitude functions for each atom pair or MS path. (Complete structure refinements were not available for all the model compounds.) At a minimum, FEFF6 requires atomic coordinates for an atom cluster, a value for S_0^2, which is a many-body amplitude reduction term, and a value for a global σ^2 (defaults for the latter two can be used). We used atomic coordinates from XRD for a 7 Å radius cluster (the center assigned to a U atom), set $S_0^2 = 1.0$ initially, and chose an initial global σ^2 value of 0.003 Å^2. The global σ^2 value provided approximate scaling of multiple paths as a function of k, which allowed qualitative comparison of theoretical with experimental EXAFS spectra. The theoretical spectra used for comparison included all paths predicted to be significant by FEFF6, using the default, low-amplitude cutoff value. Where qualitative agreement was good, theoretical EXAFS spectra were calculated for individual paths. The global σ^2 value was effectively reset to zero for each path's spectrum before extraction of individual path phase-shift and amplitude functions.

Each experimental spectrum was fitted without further refinement (e.g., deglitching) using a least-squares algorithm. First, we fitted individual coordination shell information to filtered data to establish "seed" values of S_0^2, R, and σ^2. Filtered data were extracted using a Gaussian window. Because of the significant overlap of interatomic distances in the equatorial plane around U, FT features between and sometimes including O_{eq} and U could not be isolated. Values of N for all shells were fixed to known crystallographic values because of their high degree of correlation with S_0^2 and σ^2. The energy shift term, ΔE_0, which accounts for the difference between the threshold Fermi level of an electron gas (the energy reference used by FEFF6) and the actual threshold energy associated with the atom cluster being studied and is highly correlated with R, was allowed to adjust freely in the single-

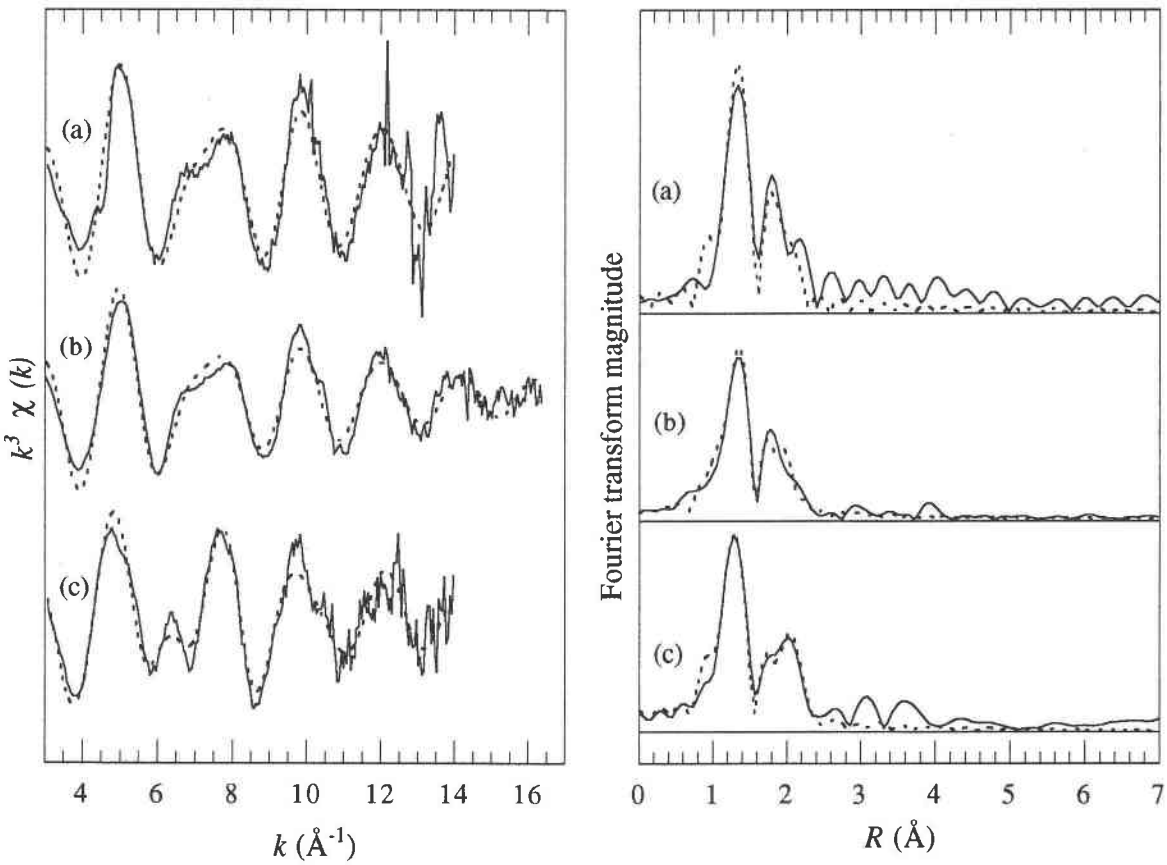

FIGURE 2. EXAFS (left) and FT (right) spectra for (**a**) aqueous uranyl monomer, (**b**) uranyl diacetate, and (**c**) uranyl nitrate. Solid lines are experimental spectra, dashed lines are fits corresponding to parameters in Table 1. FT peak positions are not corrected for phase shifts.

shell fits provided R did not deviate significantly from crystallographic values.

Values of R and σ^2 from each filtered data fit were used as seed values in a multi-shell fit of the unfiltered spectrum. The value of S_0^2 was fixed to the average of values obtained in filtered data fits (1.0). This is consistent with the finding of Li et al. (1995) that S_0^2 is approximately constant for a given absorber element in similar chemical environments. A single value of ΔE_0 for all shells was allowed to vary, in accordance with the finding that ΔE_0 is primarily a function of the absorbing atom and therefore should be approximately the same for all shells (O'Day et al. 1994). We tested this last point by allowing a separate ΔE_0 for U backscatterer shells to vary independently of ΔE_0 for all other shells. Although this improved the appearance of the fit to the FT slightly, the improvement was not significant given the increased number of variables (see goodness-of-fit parameter section), so we retained the practice of using a single ΔE_0 value. Values of N were fixed to their crystallographic values, while R and σ^2 were allowed to vary to arrive at a best fit of the data. In cases where a shell being fitted occurred in a frequency region in which other atoms were contributing to the spectrum, we sometimes fixed the R value for the shell to its crystallographic value to prevent it from attempting to account for other atoms.

The fits were not limited to shells that we had filtered, rather, we attempted to fit every spectral feature using single- and multiple-scattering paths or, where necessary, groups of paths. For shells that were not fitted to filtered data, we fixed N to the crystallographic value (for MS paths, N was allowed to vary) and allowed R and σ^2 to vary. The decision to include a shell in a final fit considered the visual quality of the fits to the EXAFS and FT spectra but was ultimately predicated on reduction of ϵ^2, the goodness-of-fit parameter.

Goodness-of-fit parameter estimation

To evaluate the improvement (or lack thereof) afforded by additional shells in fits to experimental data, we calculated relative goodness-of-fit parameters for successive fits of each spectrum in the form of a normalized χ^2 value, ϵ^2, where

$$\epsilon^2 = \frac{P_i}{\nu n} \sum_{i=1}^{n} (\text{Data}_i - \text{Model}_i)^2. \quad (1)$$

P_i is the number of independent data points given by $(2\Delta k \Delta R/\pi) + 2$, Δk is the Fourier transform range, ΔR is

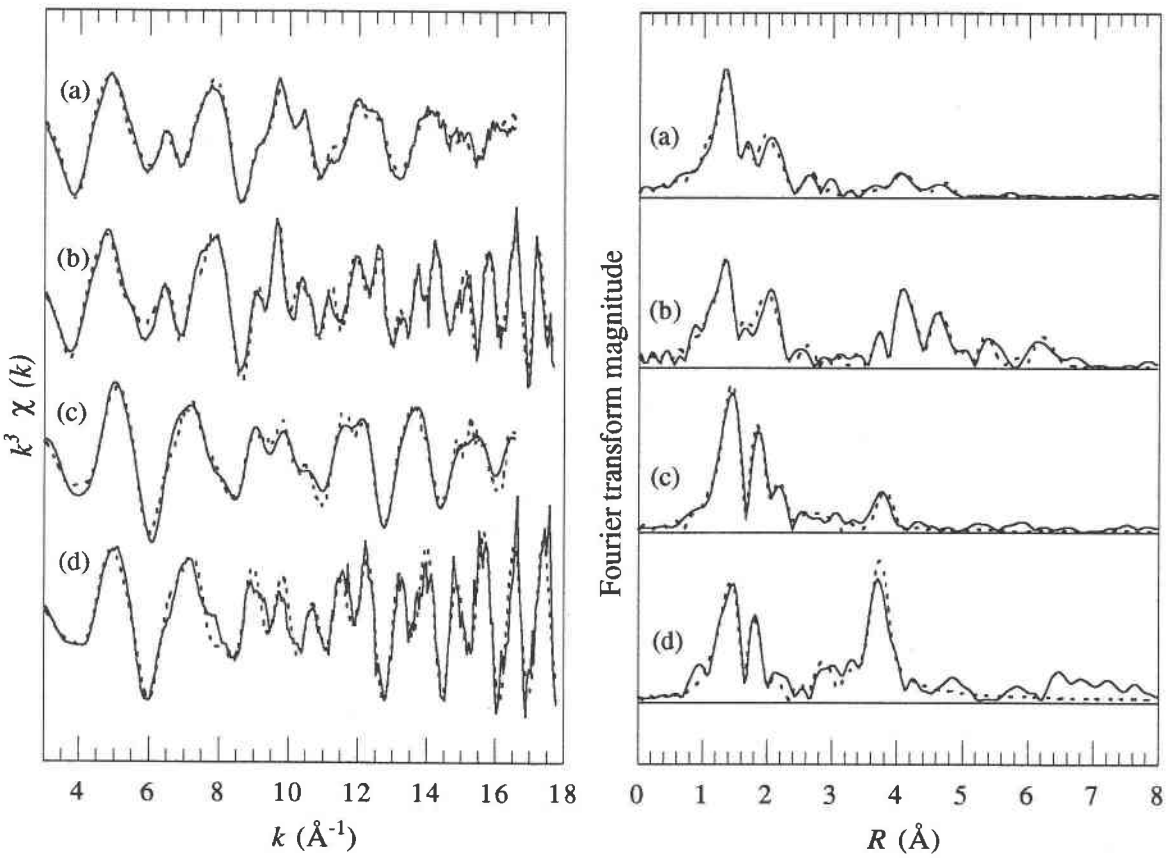

FIGURE 3. EXAFS (left) and FT (right) spectra for (**a**) rutherfordine, (**b**) rutherfordine (10 K), (**c**) uranophane, and (**d**) uranophane (10 K). Solid lines are experimental spectra, dashed lines are fits corresponding to parameters in Table 1. FT peak positions are not corrected for phase shifts.

as defined by Stern et al. (1995), ν is the degrees of freedom given by $P_i - p$, p is the number of fit parameters, n is the number of experimental data points, and (Data$_i$ − Model$_i$) is the difference between the experimental data ($k^3\chi$) and calculated fit ($k^3\chi$) for each point i. This approach differs from that taken by O'Day et al. (1994) only in the calculation of P_i (they used an approximation), for which our treatment is consistent with that of Stern et al. (1995). Our calculations of a goodness-of-fit parameter differs from that of Stern et al. (1995) by neglecting division by the standard deviation of individual experimental data points (their s_i^2). Because we only used our ϵ^2 parameter to compare fits of a single dataset, for which s_i^2 does not vary, including s_i^2 in the calculation would not alter our interpretation.

Because the ϵ^2 value reported for each shell is indicative not only of that shell's ability to fit the data, but also that of all other (typically less distant) shells already included in the fit, the ϵ^2 value is necessarily reflective of the order in which shells are added to the fit. For this reason, we followed a consistent order, adding shells that obviously contributed to the spectrum in order of increasing distance from U, followed by "backfilling" with less significant contributors. Shells of backscattering atoms are reported in Table 1 in the order in which they were added to the fit.

RESULTS AND DISCUSSION

FEFF6

Plots of FEFF6-calculated spectra superimposed on experimental spectra for uranyl nitrate and rutherfordine demonstrate the range in quality of agreement between FEFF6 and experimental spectra (Fig. 5). Whereas all major and most minor oscillations are reproduced by FEFF6 for uranyl nitrate, albeit with some amplitude discrepancies, there is poor agreement for rutherfordine.

Some discrepancy can be readily explained. The value of ΔE_0, discussed in the experimental section, was not accounted for in superimposing the spectra. On the basis of values determined while fitting the data, ΔE_0 could be as large as 6 eV, which would shift the low-k end of the EXAFS spectrum by as much as 1 Å^{-1} (Li et al. 1995). This may be relevant to the differences between rutherfordine spectra.

The use of a global Debye-Waller factor (σ^2 = 0.003 Å^2) in FEFF6 is certainly responsible for some of the observed discrepancies. As we demonstrate later in this

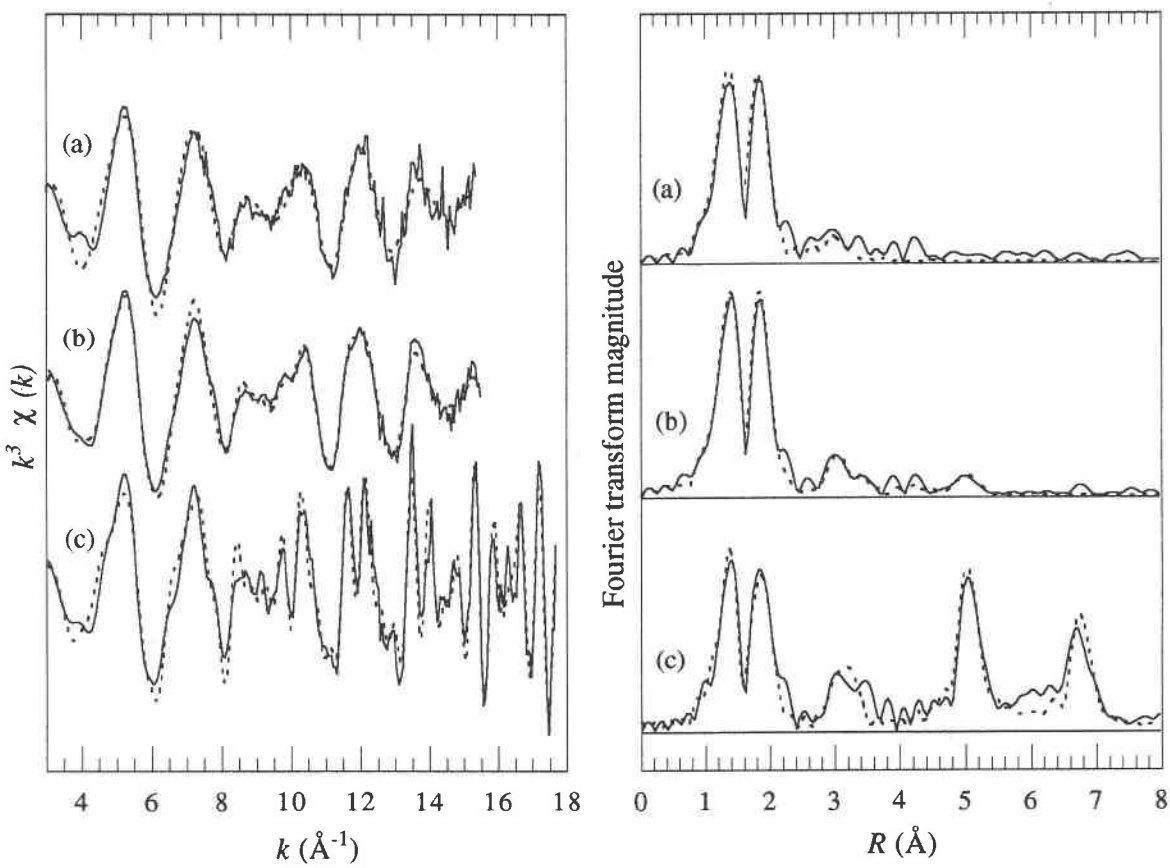

FIGURE 4. EXAFS (left) and FT (right) spectra for (**a**) meta-autunite, (**b**) meta-ankoleite, and (**c**) meta-ankoleite (10 K). Solid lines are experimental spectra, dashed lines are fits corresponding to parameters in Table 1. FT peak positions are not corrected for phase shifts.

paper, path-dependent σ^2 values for most shells, but particularly at longer distances, are larger than 0.003 Å^2, making spectral contributions smaller than those predicted by our FEFF6 calculations. Eliminating this source of discrepancy would require assignment of realistic, path-dependent σ^2 values to each path (25 to 60 paths for each FEFF6 spectrum in Fig. 5). We ascertained path-dependent σ^2 values by fitting experimental data for model compounds as part of this study, but this technique is only possible for FT features that can be isolated, typically limiting σ^2 determination to single-scattering paths corresponding to the nearest few neighbors. Although these constitute a significant part of the EXAFS signal, other paths clearly contribute, as will be demonstrated.

The quality of the structural refinement on which FEFF6 calculations are based can affect the FEFF6 spectrum dramatically. Poor structure refinements are not uncommon for U-containing crystalline materials, because the most commonly used tool is XRD, and U absorbs X-rays strongly. This absorption can be difficult to account for properly. As we discuss later, a poor structure refinement for rutherfordine is responsible for much of the discrepancy observed in Figure 5b.

Although we could repeat this qualitative comparison, additionally accounting for ΔE_0 and estimating some path-dependent σ^2 values, we feel that the excellent potential of FEFF6 for calculating EXAFS spectra (and therefore phase-shift and amplitude functions) of uranyl compounds is demonstrated in the uranyl nitrate spectra comparison. Instead, we extracted individual path phase-shift and amplitude functions from each of our four FEFF6 calculations for use in quantitative analysis of our data. In fitting the data, we treated both ΔE_0 and σ^2 as adjustable parameters to address the issues raised above. Quantitative analysis of experimental data serves as a further test of the ability of FEFF6 to model U EXAFS.

Quantitative analysis of EXAFS data

Using FEFF6-calculated phase shift and amplitude functions, we were able to account for most spectral features in our fits of experimental EXAFS data (Figs. 2–4). In the following, we address the fit to experimental data for each model compound individually. We report fit parameters in Table 1, including a comparison of interatomic distances (corrected for phase shift) with crystallographic data. Agreement between EXAFS- and XRD-derived distances is generally within ±0.02 Å; exceptions are noted below. We also report a relative good-

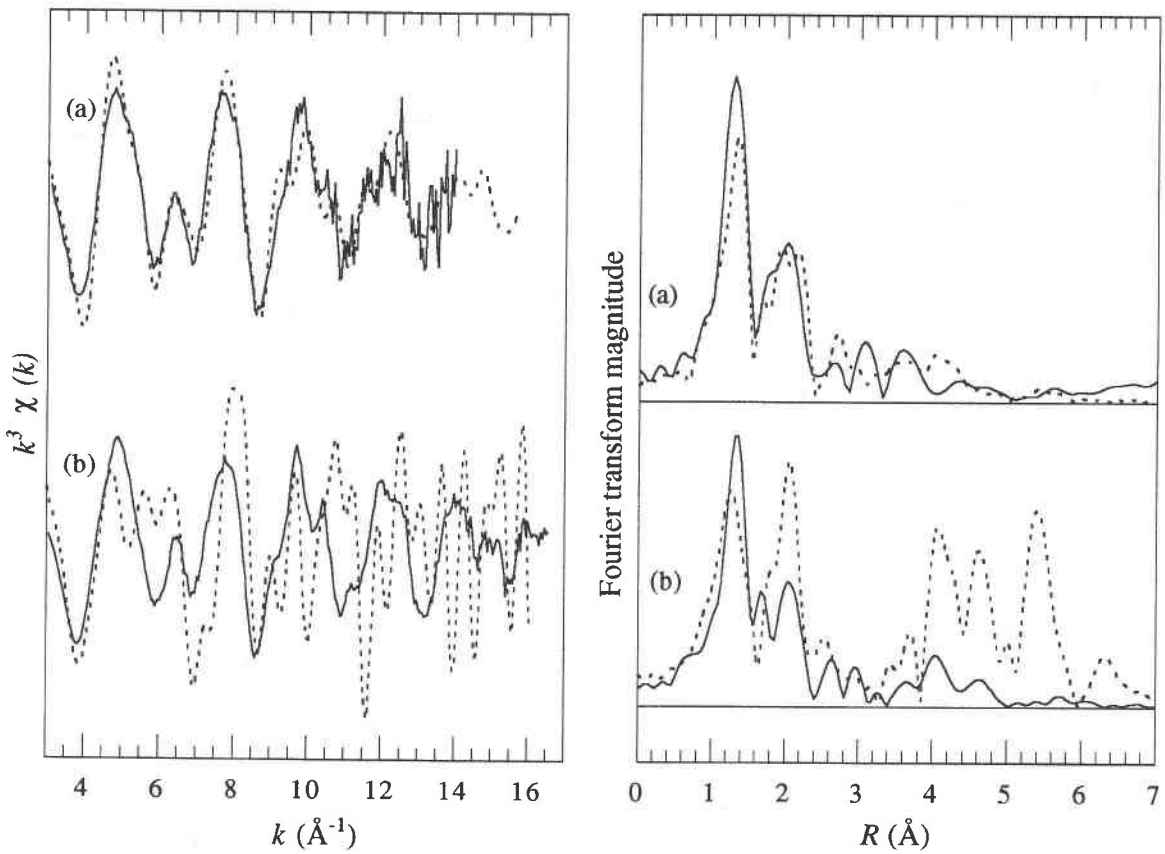

FIGURE 5. Overlay of FEFF6-calculated spectra (dashed lines) on corresponding experimental spectra (solid lines) for (**a**) uranyl nitrate and (**b**) rutherfordine: EXAFS (left); FT (right). Agreement between spectra is much better in (**a**), for which positions of most spectral features are correct but some feature amplitudes are skewed. Discrepancies between (**b**) spectra are largely attributable to the poor structure refinement on which the FEFF6 calculation is based.

ness-of-fit parameter, ϵ^2, for each successive shell added to the fit. In general, the value of ϵ^2 decreased as each shell was added, suggesting that the last-added shell improved the fit by a greater amount than can be attributed solely to the addition of adjustable parameters. Fourier transform features in the text and figures are uncorrected for phase shifts. Disorder parameters (σ^2) are discussed in a separate section.

Aqueous uranyl monomer. The aqueous uranyl monomer [$UO_2^{2+}\cdot 5H_2O$(aq)] consists of a uranyl moiety surrounded by five equatorial H_2O molecules of solvation (Görller-Walrand and Colen 1982). All the major oscillations and FT features are accounted for by a fit that consists of O_{ax} and O_{eq} contributions (Fig. 2). We were unable to account for the peak shoulder at 4.4 Å^{-1} in the EXAFS spectrum by deglitching, which we thought was the most likely cause given its shape. The peak shoulder at 7.0 Å^{-1} is not entirely accounted for, but without further structural information, we do not speculate about its origin. Fourier transform features beyond 2.3 Å cannot be distinguished from artifacts of the transform function and noise.

Our results are in good agreement with the limited structural information available for similar solution species. Both of our R values are within 0.04 Å of corresponding distances reported by another EXAFS study for a solution prepared under similar conditions (Chisholm-Brause et al. 1994). In more concentrated aqueous solutions, Åberg (1969, 1970, 1971) has found similar U-O_{ax} and U-O_{eq} distances ($R_{U\text{-}O_{ax}}$ and $R_{U\text{-}O_{eq}}$, respectively) for multimeric solution uranyl species using conventional X-ray scattering techniques. Finally, as can be seen in Table 1, our R values for the aqueous ion fall in the general range of uranyl distances in solids, as determined by XRD.

Uranyl diacetate. Uranyl diacetate [$UO_2(CH_3CO_2)_2\cdot nH_2O$] consists of a uranyl moiety with six O_{eq} atoms, four of which belong to two bidentate acetate groups and two of which are part of two H_2O molecules. Longer-range structure has not been reported. Most of the major EXAFS features are accounted for by a two-shell (O_{ax} and O_{eq}) fit, with the exception of the oscillation shoulder at 7.0 Å^{-1} and FT peaks at 3.0 and 3.9 Å (Fig. 2). Uranyl diacetate is expected to have structure beyond the O_{eq} atoms that might contribute to the EXAFS spectrum, including two C atoms approximately 2.85 Å from U [on

the basis of the structure of sodium uranyl triacetate (Templeton et al. 1985)], but these do not correspond to FT peak positions, nor does their inclusion improve the fit. In the absence of a complete structural refinement, we were unable to discern what is lacking in our fit of the experimental spectrum or to assess the possible significance of MS paths that involve atoms more distant than O_{eq}. We found that MS paths including only the central U, O_{ax}, and O_{eq}, are insignificant, however.

Mentzen and Giorgio (1970) reported interatomic distances of 1.72 Å ($R_{U\text{-}O_{ax}}$), 2.50 Å ($R_{U\text{-}O_{eq}}$, acetate), and 3.0 Å ($R_{U\text{-}O_{eq}}$, water) for uranyl diacetate. Their first distance is somewhat shorter and their last distance is so much longer than similar distances in other uranyl compounds that we doubt their validity, thus we have not included them in Table 1 for comparison. Our EXAFS-derived $R_{U\text{-}O_{ax}}$ value is in good agreement with that for sodium uranyl triacetate (1.758 Å), but our $R_{U\text{-}O_{eq}}$ value is significantly shorter than the 2.464 Å in sodium uranyl triacetate. This is not unreasonable, given that two of the equatorial ligands in uranyl diacetate are H_2O molecules, which tend to have significantly shorter $U\text{-}O_{eq}$ distances (closer to 2.30 Å) than acetate. Grouped with $U\text{-}O_{eq}$ bond lengths for acetate, the H_2O ligands would cause a shorter average EXAFS-derived $R_{U\text{-}O_{eq}}$ value for uranyl diacetate than that found for sodium uranyl triacetate.

Uranyl nitrate. Uranyl nitrate [$UO_2(NO_3)_2 \cdot 6H_2O$] consists of a uranyl moiety surrounded by six O_{eq} atoms, four of which belong to two bidentate nitrate groups and two of which are part of two H_2O molecules (Fig. 1a) (Taylor and Mueller 1965). Longer-range structure has not been proposed for this species.

All major EXAFS oscillations are accounted for by a three-shell (O_{ax}, O_{eq}, and N) fit (Fig. 2). Judging from its relative ϵ^2 value, the N shell is not a significant contributor to the fit. Minor EXAFS oscillations that were not fitted probably correspond to FT features at 3.1 and 3.6 Å, which do not coincide with any atoms in the uranyl nitrate structure. This suggests that these peaks may be due to multiple scattering.

To evaluate MS in the uranyl nitrate structure, we carried out a FEFF6 calculation that included all paths deemed significant by FEFF6. Despite the use of a global σ^2 value, the calculation predicted a FT peak at 3.6 Å, albeit with an incorrect magnitude (Fig. 5). Of the 22 MS paths with effective distances between 3.3 and 3.7 Å, linear three- and four-leg paths between U and one or both of its axial O atoms are predicted by FEFF6 to have the largest amplitudes, but the corresponding FT features peak at 2.9 Å, where there is no feature in our experimental spectrum. The next strongest contributions are predicted to arise from linear scattering among the U, N, and terminal nitrate-O atoms; the corresponding FT feature peaks at 3.6 Å, thus contributing amplitude to one of the two neglected peaks. Nine different types of MS paths have effective distances between the two just described, each with similar order-of-magnitude FEFF6 amplitudes. Of the nine, adding only those paths with the highest amplitudes to the existing three-shell fit does not account for the FT feature at 3.1 Å. Adding all nine paths with their σ^2 values fixed to 0.003 Å^2 results in a nearby FT peak with an incorrect amplitude, suggesting they may all contribute but should have different σ^2 values. Individually adjusting each N and σ^2 value would leave the system underconstrained, however. We conclude that the FT peaks at 3.1 and 3.6 Å result from complex interference among several MS paths. The absence of MS paths from the three-shell (single-scattering) fit has apparently not affected the values of parameters resulting from the fit; interatomic distances are within 0.02 Å of crystallographic values (Taylor and Mueller 1965) for all three shells.

Rutherfordine. The rutherfordine structure (UO_2CO_3) consists of uranyl moieties surrounded by six O_{eq} atoms, four of which belong to two bidentate carbonate groups and two of which belong to two monodentate carbonate groups (Cromer and Harper 1955). Each carbonate O_{eq} atom is shared by two uranyl groups, which form the basis for a sheet-like structure. Stacking of the layers is believed to occur with some disorder, such that interatomic distances may vary from one layer to the next (Christ et al. 1955).

All major and minor rutherfordine EXAFS oscillations are reproduced by a fit consisting of contributions from O_{ax}, O_{eq}, C, U at two distances, and distant O (O_{dist}) atoms (Fig. 3). Contributions from O_{eq}, C, and O_{dist} shells produce the EXAFS oscillation that peaks at 6.3 Å^{-1}. Typically, distant O atoms would not be expected to contribute significant amplitude because of their weak scattering potential, but excluding the O_{dist} contribution from this fit results in a much poorer visual fit of the EXAFS spectrum in the 5.5–7.5 Å^{-1} region. Addition of the O_{dist} shell also reduces the ϵ^2 for the fit. It follows that these distant O atoms produce a more significant EXAFS contribution than one might expect because they are axial to neighboring U atoms; therefore their positions are stabilized by the strong $U\text{-}O_{ax}$ bond (in other words, their vibrational disorder is low). Furthermore, eight O atoms coincide at a single distance to contribute significant amplitude.

EXAFS-derived R values are in relatively poor agreement with XRD values (Cromer and Harper 1955), particularly for $R_{U\text{-}O_{ax}}$ and $R_{U\text{-}O_{dist}}$. We suspect the XRD values are incorrect because the XRD $R_{U\text{-}O_{ax}}$ is significantly shorter than similar distances in other uranyl compounds, and for reasons described in the preceding paragraph, $R_{U\text{-}O_{ax}}$ affects $R_{U\text{-}O_{dist}}$. Furthermore, stacking disorder may account for a real difference in R values measured by the two techniques. We discuss these discrepancies further in a later section of this paper.

Low-temperature rutherfordine. An eight-shell fit accounts for all major EXAFS oscillations and FT peaks in the rutherfordine spectrum collected at 10 K (Fig. 3). In addition to the six shells fitted to the ambient-temperature spectrum, we fitted two more distant U shells (U3 and U4) to the 10 K spectrum. Contributions by U3 and U4 are clearly indicated by structure in the high-k region

of the EXAFS spectrum as well as FT features at 5.3 and 6.3 Å. Minor discrepancies between the fit and the experimental spectrum are primarily in the low-k region, where MS and other complex interactions that are difficult to account for are expected to play a greater role.

Unlike the ambient-temperature ϵ^2 value, the 10 K ϵ^2 value associated with the C shell is larger than the previous ϵ^2 value, suggesting that the significance of the C shell has dropped at low temperature. This and the detection of U3 and U4 are probably attributable to two factors: dampened vibrational disorder at low temperature, which results in stronger contributions from distant atoms (e.g., U) (causing the C shell to become relatively less significant) and the k^3 weighting factor in Equation 1, which weights shells with large scattering amplitudes at higher k values (such as U) more heavily. Discrepancies between EXAFS- and XRD-derived interatomic distances are similar to those discussed for the ambient-temperature rutherfordine spectrum.

Uranophane. Uranophane $[Ca(UO_2)_2(SiO_3OH)_2 \cdot 5H_2O]$ is a 1:1 uranyl silicate mineral that consists of uranyl moieties in fivefold equatorial coordination. Uranyl pentagons form a continuous edge-sharing chain; chains are linked to form sheets by silicate tetrahedra (Fig. 1b). Parallel uranyl silicate sheets make up the uranophane structure, with Ca^{2+} ions between the layers. Two uranophane structures (α and β) have been reported (Viswanathan and Harneit 1986; Ginderow 1988); their crystallographic parameters differ slightly (Table 1).

A four-shell (O_{ax}, O_{eq1}, O_{eq2}, and U) fit of uranophane EXAFS data results in an excellent reproduction of virtually all oscillatory features (Fig. 3). Resulting interatomic distances agree within ±0.04 Å for all four shells with both reported structures, although agreement with the β-structure is slightly better. Unlike spectra for the other model compounds in this study, the uranophane O_{eq} shell is split into two subshells, as determined by a lower ϵ^2 value than that associated with a single O_{eq} shell. Although crystallographic U-O_{eq} distances are not clearly separated into two groups, they span an R range large enough to be discerned as two separate peaks in an EXAFS spectrum for which $\Delta k = 11$ Å^{-1} (or greater, as it is here), in accordance with $\Delta R \geq \pi/2\Delta k$.

Despite the high quality of the four-shell fit, a distinct feature at 12 Å^{-1} is not accounted for, and FT features between 2.5 and 3.5 Å are not properly fitted. The fit does not include atoms located between O_{eq} and U (at 3.9 Å), namely four Si atoms [3.14, 3.63, 3.75, and 3.78 Å (Ginderow 1988)]. Adding one Si atom at 3.17 Å improves the fit (ϵ^2 decreases), but additional Si atoms do not improve the fit. The four shortest U-Si distances in the uranophane structure appear to lie at the borderline of detection by EXAFS, and because they are all different, the resulting spectra interfere destructively to preclude detection of all but the closest Si. Furthermore, according to FEFF6 calculations, several higher amplitude MS paths have total path lengths that are interspersed with single scattering to Si atoms. The "complete" FEFF6 calculation, which includes all four Si atoms as well as several MS paths, does reproduce the feature at 12 Å^{-1} and its FT matches that of the experimental data remarkably well (not shown). Given the low symmetry of the U site in uranophane, however, we would not expect MS contributions to be large.

Low-temperature uranophane. The same five shells of atoms were fitted to the uranophane spectrum collected at 10 K. The five-shell fit accounts for most spectral features, with the exceptions of an oscillation shoulder at 7.9 Å^{-1} and some fine structure between 8.5 and 10.5 Å^{-1} in the EXAFS spectrum (Fig. 3). Both of these are probably related to the absence of more distant Si atoms from the fit, because the Si amplitude envelope is highest in this range of k values. Adding another Si shell does not improve the fit, however, possibly because other paths that are absent from the fit contribute to the spectrum in the same region and therefore mask the Si contribution. Several FT features above 4.5 Å appear to be significant and may correspond to more distant U neighbors (6.02 and 6.66 Å), but their inclusion does not improve the fit, visually or by reducing ϵ^2. The absence from the fit of lesser single-scattering paths or, more likely, MS paths with a similar frequency to the more distant U neighbors, likely accounts for this lack of improvement.

Unlike the ambient-temperature fit, the second O_{eq} subshell does not improve the low-temperature fit (ϵ^2 increases). This is likely attributable to the lower proportional amplitude of closer, lighter atoms at low temperature owing to the increased amplitude of more distant, heavier atoms. Low-temperature $R_{U\text{-}O_{eq}}$ values are notably shorter than similar values derived from ambient-temperature data. In fact, with the exception of $R_{U\text{-}Si}$, the determination of which is probably less precise by XAFS because it lies in a more cluttered spectral region, our low-temperature interatomic distances are more consistent with crystallographic distances reported for α-uranophane than for β-uranophane, suggesting that the shift to low temperature may have effected a displacive structural transformation. Agreement with α-uranophane R values is within ±0.03 Å for four of the shells, ±0.05 Å for Si.

Meta-autunite. Meta-autunite $[Ca(UO_2)_2(PO_4)_2 \cdot 6H_2O]$ is a 1:1 uranyl phosphate mineral in which each uranyl moiety is surrounded by four O_{eq} atoms, each of which occupies one corner of a phosphate tetrahedron (Smith 1984). The uranyl phosphate network extends to form sheets, between which Ca^{2+} ions are located. A two-shell (O_{ax} and O_{eq}) fit accounts for all of the major EXAFS oscillations, but only the two lowest R FT peaks. There appears to be fine structure between 8.5 and 10.5 Å^{-1} that is reproduced by FEFF6, but the noise level in the data largely obscures the features. Fourier transform peaks between 2.5 and 3.5 Å appear to stand above the noise level but are not accounted for by the two-shell fit. The addition of a P shell to the fit accounts for the dominant peak, located at 3.1 Å, but it does not significantly improve the fit in the 8.5–10.5 Å^{-1} region, nor does it affect ϵ^2 dramatically (Fig. 4). In addition to O_{ax}, O_{eq}, and P paths,

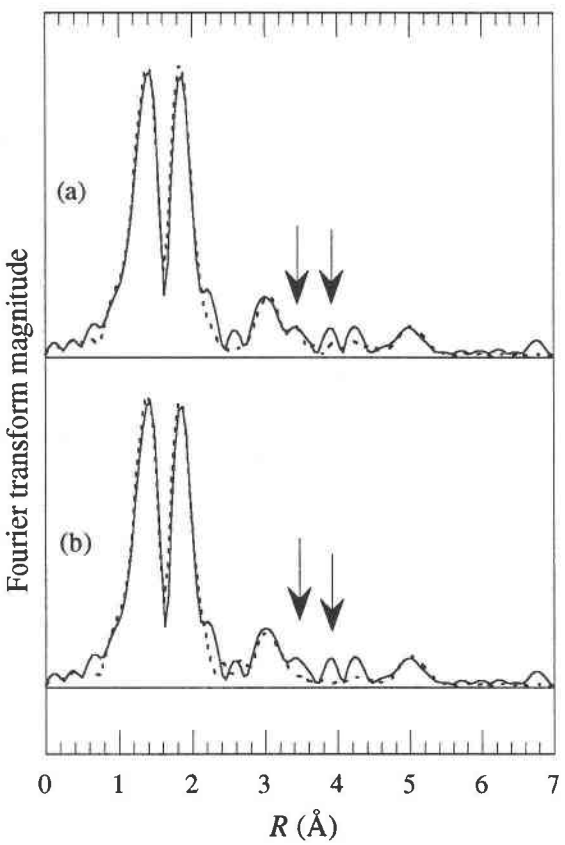

FIGURE 6. Meta-ankoleite FT spectrum fit (**a**) with and (**b**) without the MS paths indicated in Table 1. Solid line is the experimental spectrum; dashed line is the fit. Single-scattering paths are the same in both fits. Areas of minor improvement afforded by including the MS paths are denoted in this figure by arrows.

the FEFF6 calculation predicts significant amplitude for distant O (four at 3.88 Å and four at 4.11 Å) and several MS paths. Multiple-scattering contributions should be more significant for meta-autunite (and meta-ankoleite) than for the other structures addressed in this study owing to the higher symmetry of the U site in meta-autunite and meta-ankoleite. We were not successful in accounting for the remaining features by including additional shells for single- or multiple-scattering paths in the fit, but we suspect that the complexity that results from having several overlapping paths combined with lessened resolution owing to spectral noise, rather than insignificance of the paths, is to blame.

Meta-ankoleite. Meta-ankoleite $[K_2(UO_2)_2(PO_4)_2{\cdot}6H_2O]$ is isostructural with meta-autunite, with K^+ rather than Ca^{2+} ions occupying the interlayer region. All the features described for meta-autunite are present in the meta-ankoleite spectra, although with a higher signal-to-noise ratio. A three-shell (O_{ax}, O_{eq}, and P) simulation of meta-ankoleite data is very similar to the one for meta-autunite in its ability to fit spectral features, but the fit's shortcomings

TABLE 2. Shell-dependent disorder parameters (σ^2)

Atom	*N*	*R* (Å)	σ^2 (Å^2)
O_{ax}	2	1.76–1.82	0.0015–0.0040
O_{eq}	4–6	2.28–2.49	0.0025–0.0127
N	2	2.93	0.0101
C	2	2.94	0.0024
Si	1	3.17	0.0033
P	4	3.60	0.0043–0.0153
O_{dist}	8	4.28	0.0097
U1	2	3.96–4.31	0.0054–0.0061
U1	4	5.25	0.0093
U2	2	4.88	0.0064

are more apparent for meta-ankoleite because of the higher quality data. The addition of a U neighbor shell at 5.24 Å to the fit accounts for most of the fine structure in the 8.5–10.5 Å^{-1} region that remained unaccounted for in the meta-autunite fit.

To improve the FT fit in the 3–5 Å range, we included two MS paths in the fit, one corresponding to near linear scattering off an O_{eq} on the return path from P and the other consisting of a "path group" of four different (single- and multiple-scattering) paths with nearly identical path lengths. These two shells improve the fit, particularly in the 3.0–4.0 Å range (Fig. 6). Clearly other paths contribute to the spectrum as evidenced by unfit features, but with another 20+ single- and multiple-scattering paths that have effective distances in this region, it is neither reasonable nor worthwhile to attempt to include them. We included two MS paths here simply to demonstrate their minor but apparent contribution to the EXAFS spectrum of a highly symmetrical uranyl structure.

Low-temperature meta-ankoleite. Six shells make up the 10 K meta-ankoleite fit, including the four single-scattering shells used to fit the ambient-temperature meta-ankoleite spectrum, a more distant U shell (U2), and a path group of four MS paths that overlap considerably with U2 (Fig. 4). The U2 shell parameters could not be refined in the absence of the MS path group, presumably because of the extremely high correlation between the two. The fit has some shortcomings, probably owing to the multitude of MS paths, mentioned above, that have not been included in the fit.

Disorder parameters

The σ^2 values derived from ambient-temperature data for similar backscattering shells vary little among the seven model compounds; trends within each type of shell are consistent with what one might expect on the basis of coordination number and static disorder (Table 2). Values of σ^2 for the U-O_{ax} bond lie between 0.0015 and 0.0040 Å^2. The larger values are found for those compounds (meta-autunite, meta-ankoleite) in which the relevant static disorder (difference between the two U-O_{ax} bond lengths) is relatively large. For compounds in which the O_{eq} atoms were fitted as a single shell (all except uranophane), U-O_{eq} σ^2 values lie between 0.0025 and 0.0127 Å^2. While this range is relatively large, the lower values

are for meta-autunite and meta-ankoleite, for which lower σ^2 values would be expected because they have the smallest number of O_{eq} neighbors (four) with the least static disorder. Without meta-autunite and meta-ankoleite, the lower limit for U-O_{eq} σ^2 values increases to 0.0092 Å^2. The new low σ^2 value belongs to the aqueous uranyl monomer, in which five O_{eq} atoms are believed to be equidistant from U. More static disorder is characteristic of the O_{eq} shell of the other model compounds, hence the higher σ^2 values. For uranophane, splitting the O_{eq} shell into two subshells results in low σ^2 values (0.002 Å^2) for each subshell, consistent with small coordination number and relatively low static disorder within each subshell. Finally, values of σ^2 for U shells are 0.005–0.006 Å^2 for N = 2 (rutherfordine and uranophane) and 0.009 Å^2 for N = 4 (meta-ankoleite).

With the exception of uranophane, the primary effect of lowering the temperature to 10 K was to reduce σ^2 values slightly, if at all. Because vibrational disorder should be fully damped at 10 K, this suggests that most of the disorder in uranyl structures at ambient temperature is static, or positional. If we believe the XRD structure refinements for α- and β-uranophane, then it appears that lowering the temperature to 10 K effected a displacive reconstruction of uranophane from the β to the α polymorph.

We have found no satisfactory basis for evaluation of our σ^2 values, other than their own consistency among compounds. Disorder parameters can be estimated in several ways (Scott 1984), but the theory is not well developed, especially for complicated structures such as those containing the uranyl moiety. Uranyl environment σ^2 values have been derived by fitting EXAFS spectra for similar systems by other authors, but these have generally been for structures much less well constrained than model compounds, thus N was simultaneously adjusted in the fitting process (Chisholm-Brause et al. 1994; Combes 1988; Dent et al. 1992; Farges et al. 1992). They are not suitable for comparison because of the high correlation between N and σ^2.

Structural implications of XAFS analysis

On the basis of our quantitative analysis of experimental EXAFS spectra, we suspect that two uranyl compound structure refinements are incorrect. The only uranyl diacetate structure report we could find was that by Mentzen and Giorgio (1970). In comparison with many uranyl structures, their $R_{U\text{-}O_{eq,water}}$ value of 3.0 Å is too long to be realistic (Weigel 1986). Our average $R_{U\text{-}O_{eq}}$ value of 2.40 Å for this compound is more consistent with characteristic bond lengths, as discussed earlier in the uranyl diacetate analysis section. We therefore propose that the correct structure for uranyl diacetate is consistent with the average interatomic distances determined in our EXAFS analysis.

We have already raised concern about the Cromer and Harper (1955) rutherfordine refinement. In addition to reporting very large tolerances for interatomic distances (±0.09 Å for $R_{U\text{-}O_{ax}}$), their $R_{U\text{-}O_{ax}}$ value (1.67 Å) is much shorter than those of other uranyl carbonates, including potassium uranyl carbonate (1.80 Å) (Anderson et al. 1980) and aqueous triuranylhexacarbonate ion (1.80 Å) (Åberg et al. 1983). Our rutherfordine $R_{U\text{-}O_{ax}}$ value of 1.77 Å is much closer to these other uranyl carbonate $R_{U\text{-}O_{ax}}$ values. Furthermore, we are reasonably certain that our XAFS spectrum was not affected by minor impurities in our rutherfordine specimen, if any were present, because impurity phases that are common in naturally occurring rutherfordine (uraninite, becquerelite, and masuyite) (Clark and Christ 1957) would be discerned by either a shifted XAFS edge jump [uraninite contains U^{4+}] or a significantly different atomic arrangement suggested by the EXAFS spectrum.

To compare our structure with that of Cromer and Harper on another level, we can apply bond-valence calculations to both structures to estimate the valence balance at the central U atom. The bond valence model states that a bond's valence, υ_{ij}, is related to the bond length by $\upsilon_{ij} = \exp[(R_{ij}-d_{ij})/b]$, in which R_{ij} is the tabulated bond valence parameter between atoms of types i and j, d_{ij} is the distance between atoms i and j, and b is a constant (0.37 Å) (Brown and Altermatt 1985; Brese and O'Keeffe 1991). Furthermore, the sum of bond valences for all bonds to a given atom should equal that atom's formal valence, V_i, expressed as $V_i = \Sigma_{j=1}^{N}\upsilon_{ij}$ (Pauling 1929). Calculating $\Sigma\upsilon_{ij}$ for our structure and that of Cromer and Harper using R_{ij} = 2.075 Å (Brown and Altermatt 1985), we find values of 6.71 and 7.99 v.u., respectively, compared with a formal charge on U of 6.0. Although our $\Sigma\upsilon_{ij}$ value is not identical to V_U, it is much closer than the $\Sigma\upsilon_{ij}$ for the Cromer and Harper structure. This agreement, in addition to the arguments made above, favors our partial structure derived from EXAFS analysis.

Implications of findings

We have observed contributions to uranyl spectra from O_{ax}, O_{eq}, N (2.9 Å), C (2.9 Å), Si (3.2 Å), P (3.6 Å), U (4.0, 4.3, 4.9, and 5.2 Å), and distant O (4.3 Å) atoms. Of these, the closer U (4.0 and 4.3 Å) shells undeniably improve the data fits over those containing just O_{ax} and O_{eq} shells. Even in samples of unknown composition, EXAFS spectroscopy should therefore detect U neighbors within 4.3 Å of each other. This is an important finding for the application of EXAFS spectroscopy to U sorption and solution studies because of the information EXAFS can be expected to provide about U cluster and precipitate formation.

Fit improvement afforded by incorporation of the other shells that were detected in this study is less obvious, but nonetheless real (with the exception of N). This suggests that these elements (at the stated distances) would be detected in EXAFS spectra of unknown uranyl structures, if present. In reality, detection of the C, Si, P, and distant O shells is equivocal because each tends to contribute most strongly to a region of the EXAFS spectrum that is

cluttered with spectral contributions from other atoms. Depending on the geometry of a particular structure, the scattering power of these atoms may or may not be large enough to make a discernible contribution to the spectrum. The lack of fit improvement associated with the N shell suggests that similar shells of light atoms (N, C) might not be detected in EXAFS spectra of unknown uranyl structures.

In a related study of uranyl sorption by kaolinite (Thompson et al. 1997), we observed contributions to uranyl EXAFS spectra from Si or Al atoms, or both, located 3.3 Å from U, indicating inner-sphere complexation of U by kaolinite. It is likely that the relative asymmetry of the solid-water interface precludes the multiplicity of single- and multiple-scattering paths that we occasionally found to interfere with U-Si or U-P single scattering in our more ordered model compounds of this study.

Within the limits established by the most distant atoms that were detected at ambient temperature (U, 5.2 Å), we were unable to fit contributions from O atoms at various distances and more distant Si atoms (3.6 to 3.8 Å). The former is not particularly surprising given the fairly weak scattering of O atoms, particularly beyond the first shell or two of neighbors. In the case of Si, features were present in the FT in the vicinity where we expect to find Si on the basis of known interatomic distances, but the overlap of several single- and possibly multiple-scattering path lengths resulted in our inability to fit the features explicitly. From this we conclude that scattering from Si (and Al and P, because of similar atomic number) at distances greater than 3.6 Å in uranyl structures is difficult, though not necessarily impossible (depending on the structure), to detect using EXAFS spectroscopy. This suggests that EXAFS spectra would not contain U-Si (or U-Al or U-P) features confirming outer-sphere sorption of U on aluminosilicate or phosphate minerals.

Destructive interference among MS paths precludes any path or group of paths from amassing significant amplitude relative to dominant single-scattering paths, although minor spectral features nonetheless result from MS paths, as found by Hudson et al. (1996). Consequently, the addition of MS contributions to a fit seldom improves the fit in a statistically significant fashion. In contrast to suggestions by Hudson et al. (1996), we consistently found that the absence of MS contributions from a fit did not lessen the accuracy of single-scattering parameters, in particular R, derived from the fit.

Acknowledgments

This research was supported under a National Science Foundation Graduate Research Fellowship. We also acknowledge financial support from U.S. DOE grant DE-FG03-93ER14347 (GEB and GAP). C. Chisholm-Brause generously provided several of the model compounds. D.E. Morris provided XRD spectra of the silicate and phosphate minerals. J.J. Rehr and F. Farges provided helpful insight into FEFF6 and U XAFS, respectively. The research and manuscript benefited from numerous discussions with P.A. O'Day. We thank the staff of SSRL for support during data collection. SSRL is supported by the U.S. DOE and the NIH.

References cited

Åberg, M. (1969) The crystal structure of $[(UO_2)_2(OH)_2Cl_2(H_2O)_4]$. Acta Chemica Scandinavica, 23, 791–810.

——— (1970) On the structures of the predominant hydrolysis products of uranyl (VI) in solution. Acta Chemica Scandinavica, 24, 2901–2915.

——— (1971) On the crystal structure of a tetranuclear hydroxo complex of uranyl (VI). Acta Chemica Scandinavica, 25, 368–369.

Åberg, M., Ferri, D., Glaser, J., and Grenthe, I. (1983) Studies of metal carbonate equilibria. 8. Structure of the hexakis(carbonato)tris[dioxouranate(VI)] ion in aqueous solution. An x-ray diffraction and ^{13}C NMR study. Inorganic Chemistry, 22, 3981–3985.

Allen, P.G., Bucher, J.J., Clark, D.L., Edelstein, N.M., Ekberg, S.A., Gohdes, J.W., Hudson, E.A., Kaltsoyannis, N., Lukens, W.W., Neu, M.P., Palmer, P.D., Reich, T., Shuh, D.K., Tait, C.D., and Zwick, B.D. (1995) Multinuclear NMR, Raman, EXAFS, and X-ray diffraction studies of uranyl carbonate complexes in near-neutral aqueous solution. X-ray structure of $[C(NH_2)_3]_6[(UO_2)_3(CO_3)_6]\cdot 6.5H_2O$. Inorganic Chemistry, 34, 4797–4807.

Anderson, A., Chieh, C., Irish, D.E., and Tong, J.P.K. (1980) An X-ray crystallographic, Raman, and infrared spectral study of crystalline potassium uranyl carbonate, $K_4UO_2(CO_3)_3$. Canadian Journal of Chemistry, 58, 1651–1658.

Brese, N.E. and O'Keeffe, M. (1991) Bond-valence parameters for solids. Acta Crystallographica, B47, 192–197.

Brown, I.D. and Altermatt, D. (1985) Bond-valence parameters obtained from a systematic analysis of the inorganic crystal structure database. Acta Crystallographica, B41, 244–247.

Brown, G.E., Jr., Calas, G., Waychunas, G.A., and Petiau, J. (1988) X-ray absorption spectroscopy and its applications in mineralogy and geochemistry. In Mineralogical Society of America Reviews in Mineralogy, 18, 431–512.

Chisholm-Brause, C., Conradson, S.D., Buscher, C.T., Eller, P.G., and Morris, D.E. (1994) Speciation of uranyl sorbed at multiple binding sites on montmorillonite. Geochimica et Cosmochimica Acta, 58, 3625–3631.

Christ, C.L., Clark, J.R., and Evans, H.T., Jr. (1955) Crystal structure of rutherfordine, UO_2CO_3. Science, 121, 472–473.

Clark, J.R. and Christ, C.L. (1957) Some observations on rutherfordine. American Mineralogist, 41, 844–850.

Combes, J.-M. (1988) Evolution de la structure locale des polymeres et gels ferriques lors de la cristallisation des oxydes de fer. Application au piegeage de l'uranium. 194 p. Ph.D. thesis, Sciences de la Terre, l'Universite Pierre et Marie Curie, Paris, France.

Cramer, S.P. and Hodgson, K.O. (1979) X-ray absorption spectroscopy: a new structural method and its applications to bioinorganic chemistry. Progress in Inorganic Chemistry, 25, 1–39.

Cromer, D.T. and Harper, P.E. (1955) The length of the uranyl ion in uranyl carbonate. Acta Crystallographica, 8, 847–848.

Dent, A.J., Ramsay, J.D.F., and Swanton, S.W. (1992) An EXAFS study of uranyl ion in solution and sorbed onto silica and montmorillonite clay colloids. Journal of Colloid and Interface Science, 150, 45–60.

Farges, F., Ponader, C.W., Calas, G., and Brown, G.E., Jr. (1992) Structural environments of incompatible elements in silicate glass/melt systems: II. U(IV), U(V), and U(VI). Geochimica et Cosmochimica Acta, 56, 4205–4220.

George, G.N. and Pickering, I.J. (1993) EXAFSPAK: A Suite of Computer Programs for Analysis of X-ray Absorption Spectra. Stanford Synchrotron Radiation Laboratory.

Ginderow, P.D. (1988) Structure de l'Uranophane alpha, $Ca(UO_2)_2(SiO_3OH)_2\cdot 5H_2O$. Acta Crystallographica, C44, 421–424.

Görller-Walrand, C. and Colen, W. (1982) On the coordination symmetry of the hydrated uranyl ion. Chemical Physics Letters, 93, 82–85.

Grenthe, I., Fuger, J., Konings, R.J.M., Lemire, R.J., Muller, A.B., Nguyen-Trung, C., and Wanner, H. (1992) Chemical Thermodynamics of Uranium. 715 p. North-Holland, Amsterdam.

Hudson, E.A., Allen, P.G., Terminello, L.J., Denecke, M.A., and Reich, T. (1996) Polarized x-ray-absorption spectroscopy of the uranyl ion: comparison of experiment and theory. Physical Review B, 54, 156–165.

Karim, D.P., Georgopoulos, P., and Knapp, G.S. (1980) Extended X-ray

absorption fine structure studies of actinide ions in aqueous solution. Nuclear Technology, 51, 162–168.

Knapp, G.S., Veal, B.W., Lam, D.J., Paulikas, A.P., and Pan, H.K. (1984) EXAFS studies of silicate glasses containing uranium. Materials Letters, 2, 253–256.

Li, G.G., Bridges, F., and Booth, C.H. (1995) X-ray-absorption fine-structure standards: a comparison of experiment and theory. Physical Review B, 52, 6332–6348.

Manceau, A., Charlet, L., Boisset, M.C., Didier, B., and Spadini, L. (1992) Sorption and speciation of heavy metals on hydrous Fe and Mn oxides. From microscopic to macroscopic. Applied Clay Science, 7, 201–223.

McMaster, W.H., Kerr del Grande, N., Mallet, J.H., and Hubbell, J.H. (1969) Compilation of x-ray cross sections. Lawrence Radiation Lab, Report UCRL-50/74.

Mentzen, B. and Giorgio, G. (1970) Caracterisaton a l'etat solide de l'acetate d'uranyle dihydrate. Journal of Inorganic and Nuclear Chemistry, 32, 1509–1516.

Morosin, B. (1978) Hydrogen uranyl phosphate tetrahydrate, a hydrogen ion solid electrolyte. Acta Crystallographica, B34, 3732–3734.

Mustre de Leon, J., Rehr, J.J., Zabinsky, S.I., and Albers, R.C. (1991) Ab initio curved-wave x-ray-absorption fine structure. Physical Review B, 44, 4146–4156.

O'Day, P.A., Rehr, J.J., Zabinsky, S.I., and Brown, G.E., Jr. (1994) Extended X-ray Absorption Fine Structure (EXAFS) analysis of disorder and multiple-scattering in complex crystalline solids. Journal of the American Chemical Society, 116, 2938–2949.

Papelis, C., Hayes, K.F., and Leckie, J.O. (1988) HYDRAQL: A program for the computation of chemical equilibrium composition of aqueous batch systems including surface-complexation modeling of ion adsorption at the oxide/solution interface. Stanford University.

Pauling, L. (1929) The principles determining the structure of complex ionic crystals. Journal of the American Chemical Society, 51, 1010–1026.

Rehr, J.J., Mustre de Leon, J., Zabinsky, S.I., and Albers, R.C. (1991) Theoretical X-ray absorption fine structure standards. Journal of the American Chemical Society, 113, 5135–5140.

Sayers, D.E. and Bunker, B.A. (1988) Data Analysis. In D.C. Koningsberger, and R. Prins, Eds. X-Ray Absorption Principles, Applications, Techniques of EXAFS, SEXAFS and XANES, p. 211–253. Wiley, New York.

Scott, R.A. (1984) X-ray absorption spectroscopy. In D.L. Rousseau, Ed., Structural and Resonance Techniques in Biological Research, p. 295–362. Academic Press, Orlando.

Smith, D.K., Jr. (1984) Uranium mineralogy. In B. DeVivo, F. Ippolito, G. Capaldi, and P.R. Simpson, Eds. Uranium geochemistry, mineralogy, geology, exploration and resources, p. 43–88. The Institution of Mining and Metallurgy, London.

Stern, E.A. (1988) Theory of EXAFS. In D.C. Koningsberger, and R. Prins, Eds., X-ray Absorption: Principles, Applications, Techniques of EXAFS, SEXAFS, and XANES, p. 3–51. Wiley-Interscience, New York.

Stern, E.A., Newville, M., Ravel, B., Yacoby, Y., and Haskel, D. (1995) The UWXAFS analysis package: philosophy and details. Physica B, 208&209, 117–120.

Taylor, J.C. and Mueller, M.H. (1965) A neutron diffraction study of uranyl nitrate hexahydrate. Acta Crystallographica, 19, 536–543.

Templeton, D.H., Zalkin, A., Ruben, H., and Templeton, L.K. (1985) Redetermination and absolute configuration of sodium uranyl (VI) triacetate. Acta Crystallographica, C41, 1439–1441.

Teo, B.K. (1986) EXAFS: Basic principles and data analysis, 349 p. Springer-Verlag, New York.

Thompson, H.A. (1994) Structure and composition of uranium(VI) sorption complexes at the kaolinite-water interface. M.S. thesis, Stanford University, Stanford, California.

Thompson, H.A., Parks, G.A., and Brown, G.E., Jr. (1997) Structure and composition of uranium(VI) sorption complexes at the kaolinite-water interface. In E.A. Jenne, Ed., Sorption of Metals by Earth Materials, in press.

U.S. Department of Energy. (1995) Estimating the cold war mortgage: the 1995 baseline environmental management report. U.S. DOE Office of Environmental Management.

Vaughan, D. (1986) X-ray Data Booklet. Lawrence Berkeley Laboratory, Berkeley, California.

Viswanathan, K. and Harneit, O. (1986) Refined crystal structure of beta-uranophane, $Ca(UO_2)_2(SiO_3OH)_2 \cdot 5H_2O$. American Mineralogist, 71, 1489–1493.

Waite, T.D., Davis, J.A., Payne, T.E., Waychunas, G.A., and Xu, N. (1994) Uranium(VI) adsorption to ferrihydrite: application of a surface complexation model. Geochimica et Cosmochimica Acta, 58(24), 5465–5478.

Weigel, F. (1986) Uranium. In J.J. Katz, G.T. Seaborg, and L.R. Morss, Eds. The Chemistry of the Actinide Elements, 1, p. 169–442. Chapman and Hall, New York.

Zabinsky, S.I., Rehr, J.J., Ankudinov, A., Albers, R.C., and Eller, M.J. (1995) Multiple scattering calculations of x-ray absorption spectra. Physical Review B, 52, 2995–3009.

Manuscript received September 9, 1996
Manuscript accepted February 7, 1997